AD-A161 048 INITIAL DEVELOPMENT OF A LASER ALTIMETER(U) NAVAL POSTGRADUATE SCHOOL MONTEREY CA J P GILIO SEP 85 1/1

UNCLASSIFIED F/G 14/2 NL

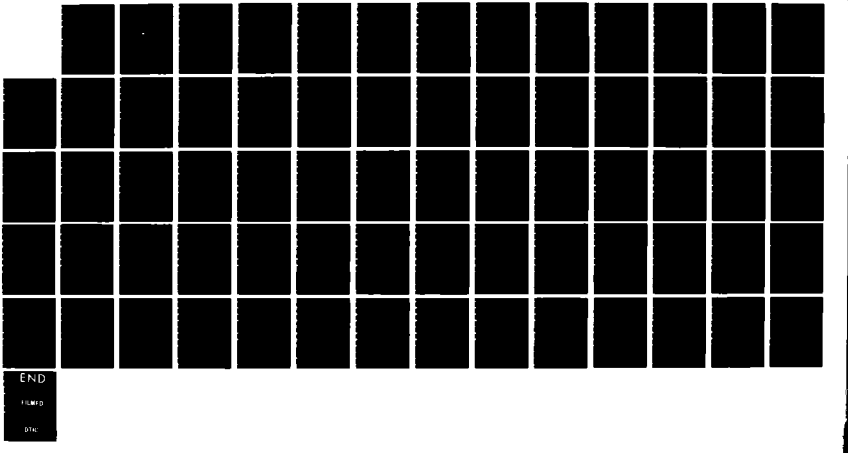

END

FILMED

DTIC

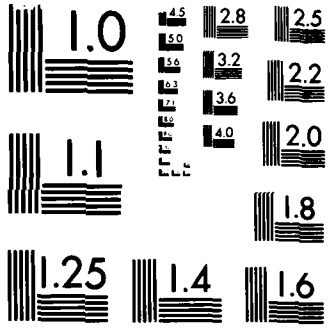

MICROCOPY RESOLUTION TEST CHART
NATIONAL BUREAU OF STANDARDS-1963-A

NAVAL POSTGRADUATE SCHOOL

Monterey, California

THESIS

INITIAL DEVELOPMENT OF A LASER ALTIMETER

by

Joseph Paul Gilio

September 1985

Thesis Advisor: A. W. Cooper

Approved for public release; distribution is unlimited.

UNCLASSIFIED

SECURITY CLASSIFICATION OF THIS PAGE (When Data Entered)

REPORT DOCUMENTATION PAGE		READ INSTRUCTIONS BEFORE COMPLETING FORM
1. REPORT NUMBER	2. GOVT ACCESSION NO. AD-A161	3. RECIPIENT'S CATALOG NUMBER 647
4. TITLE (and Subtitle) Initial Development of a Laser Altimeter		5. TYPE OF REPORT & PERIOD COVERED Master's Thesis September 1985
		6. PERFORMING ORG. REPORT NUMBER
7. AUTHOR(s) Joseph Paul Gilio		8. CONTRACT OR GRANT NUMBER(s)
9. PERFORMING ORGANIZATION NAME AND ADDRESS Naval Postgraduate School Monterey, California 93943-5100		10. PROGRAM ELEMENT, PROJECT, TASK AREA & WORK UNIT NUMBERS
11. CONTROLLING OFFICE NAME AND ADDRESS Naval Postgraduate School Monterey, California 93943-5100		12. REPORT DATE September 1985
		13. NUMBER OF PAGES 67
14. MONITORING AGENCY NAME & ADDRESS(if different from Controlling Office)		15. SECURITY CLASS. (of this report)
		15a. DECLASSIFICATION/DOWNGRADING SCHEDULE

16. DISTRIBUTION STATEMENT (of this Report)

Approved for public release; distribution is unlimited.

17. DISTRIBUTION STATEMENT (of the abstract entered in Block 20, if different from Report)

18. SUPPLEMENTARY NOTES

19. KEY WORDS (Continue on reverse side if necessary and identify by block number)

Laser, Infra-red, Altimeter

20. ABSTRACT (Continue on reverse side if necessary and identify by block number)

A design study was carried out of a small, expendable, self-contained laser altimeter for overwater operation at low altitude. A .904 μm GaAs laser was used to build a prototype transmitter/receiver at a cost of less than $600 and small enough to fit inside a 5 inch diameter cylinder, 5 inches long. Tests at a height of 120 feet above the surface of a lake resulted in a signal-to-noise ratio of 6, and

DD FORM 1 JAN 73 1473 EDITION OF 1 NOV 65 IS OBSOLETE

S N 0102-LF-014-6601

UNCLASSIFIED

SECURITY CLASSIFICATION OF THIS PAGE (When Data Entered)

validated the trade-off equation used in the study. A second test model, with design improvements incorporated, is predicted to yield a SNR of over 20 for an altitude of 150 meters. (Thesis)

Approved for public release; distribution is unlimited.

Initial Development of a Laser Altimeter

by

Joseph Paul Gilio
Lieutenant, United States Navy
B.S., University of California, 1978

Submitted in partial fulfillment of the
requirements for the degree of

MASTER OF SCIENCE IN PHYSICS

from the

NAVAL POSTGRADUATE SCHOOL
September 1985

Author: Joseph P Gilio
Joseph Paul Gilio

Approved by: A. W. Cooper
A. W. Cooper, Thesis Advisor

E. C. Crittenden, Jr.
E. C. Crittenden, Jr., Second Reader

for G. E. Schacher, Chairman, Department of Physics

John N. Dyer
John N. Dyer, Dean of Science and Engineering

ABSTRACT

A design study was carried out of a small, expendable, self-contained laser altimeter for overwater operation at low altitude. A .904 μm GaAs laser was used to build a prototype transmitter/receiver at a cost of less than $600 and small enough to fit inside a 5-inch diameter cylinder, 5 inches long. Tests at a height of 120 feet above the surface of a lake resulted in a signal-to-noise ratio of 6, and validated the trade-off equation used in the study. A second test model, with design improvements incorporated, is predicted to yield a SNR of over 20 for an altitude of 150 meters.

TABLE OF CONTENTS

ACKNOWLEDGEMENTS

I would like to express my thanks to Professor A. W. Cooper, my thesis advisor, and especially to Professors E. C. Crittenden, Jr., and G. W. Rodeback, for all the help they have provided.

This thesis was sponsored by the NATO Sea Gnat Project Office of the Space and Naval Warfare Systems Command (PDE-107-5). Support and encouragement for the project is greatly appreciated.

I. INTRODUCTION

Many methods are available for measuring height above the ocean surface. However, a small, inexpensive, system for short range determination is unavailable. Design of such a system is possible with the use of laser diodes to produce light pulses which bounce off the ocean surface. The time delay from transmission to reception determines the altitude. The many factors involved are considered below with respect to specific objectives such as size, cost, and application. These objectives define what makes one design better than another and must be kept in mind through every stage of development. This thesis covers the initial design phase for such a device and the prototype model tests.

A. BACKGROUND

The project is sponsored by the NATO Sea Gnat Project Office of the Space and Naval Warfare Systems Command (PDE-107 5) of the U.S. Navy. Efforts to improve anti-ship missile defense include research to upgrade existing defense systems. One system involves the use of chaff.

A chaff cloud, consisting of thousands of metallic strips dispersed from a ship, creates a radar cross section comparable to that of the ship. An incoming missile is then drawn toward the chaff cloud and away from the intended

target. The effectiveness of a chaff cloud depends on its position relative to the ship and its altitude. A cloud too low will disappear into the ocean before the missile is close enough to see it. A cloud too high will be too widespread when it drifts down into view. The addition of an altimeter to a chaff round can ensure the proper height of dispersion.

The altimeter must measure its distance above the sea surface. This is the design requirement. Nominal range is 150 meters. Other design objectives include:

(1) Size - It must be small enough to fit on a chaff round.

(2) Cost - one altimeter is expended with each round so unit cost must be kept low.

(3) Structural strength - It must be rugged enough to withstand the explosive launch from a ship's deck.

(4) Lifetime - Although storage life may be quite long, the operational lifetime will be only minutes.

B. PROCEDURE

To develop a system that works requires an understanding of each component and how it interrelates with the others. A trade-off equation, derived in Chapter II, determines what design parameters need to be considered and their functional dependence on signal level. Three terms of the trade-off equation correspond directly to system components; The transmitter, receiver, and detector. Each is discussed with regard to the design objectives. Also included in Chapter

II is a brief description of the overall system and the other components which become necessary during further stages of development.

The fourth term of the trade-off equation, the sea surface reflectivity, is discussed in Chapter III. Its dependence on transmitter beam pattern is determined as a function of sea state and angle of incidence. Three patterns are considered; pencil beam ($1^{o} \times 1^{o}$), offset fan-shaped beam ($1^{o} \times 10^{o}$), and wide angle beam ($20^{o} \times 20^{o}$). The analysis yields insight into a suitable beam pattern and allows performance predictions.

A prototype model was constructed using a 120 watt peak power laser diode, a 2" diameter receiver aperture, and a P-I-N photodiode detector. Details are in Chapter IV. The transition from theory to production involves further trade-offs because available rather than ideal parts are used. Laboratory tests were conducted with reflection from a plate glass window at range of 25 feet and field tests at the New Melones reservoir near Columbia, CA, from a height of 120 feet above the water surface. Results were good but less than ideal. Design improvements are being incorporated into a second model for further tests.

C. PREVIOUS WORK

Laser rangefinders have been in production for over a decade. Diverse military and civilian applications have

required a wide variety of system designs. Reference 1 discusses many of the aspects which must be considered for a specific design and how objectives, such as those listed above, affect the end product. Laser radar systems operate essentially with the same constraints as rangefinders with added features for scanning and tracking. Design techniques presented by Bachman [Ref. 2] for laser radar indicate some of the basic theory required as well as the complexities which can be avoided for simple rangefinders. The Infra-Red Handbook [Ref. 3] contains basic component design information and analysis. Most discussions emphasize increased performance for increased complexity at increased cost. The unique objectives of this laser altimeter stress reduced range and accuracy in exchange for reliability at greatly reduced cost.

The problem of the sea surface reflectivity was addressed by Swennen [Ref. 4] for a collimated light beam at normal incidence. Reflected energy levels were calculated as a function of receiver height above sea level for several transmitter-receiver spacings and receiver apertures. A similar calculation is presented in Chapter III for three divergent beam patterns and for angles of incidence up to 10^{o} from normal.

Experimental measurements of sea surface reflectivity were conducted by Stephens and Burroughs [Ref. 5]. The angle of incidence dependence was determined for several

transmitter beamwidths. Reflectivity measurements for whitecaps were simulated with a ship's wake and by spraying salt water from a fire hose. The effective reflectivity for wind speeds up to 60 knots was presented as a function of angle of incidence.

This thesis is in conjunction with an ongoing project of Professors A.W. Cooper, E.C. Crittenden, and G.W. Rodeback of the Naval Postgraduate School. They demonstrated operation of a small, "cheap" altimeter at a range of 135 meters. A 300 watt peak power gallium arsenide laser diode array was used as a transmitter. Fifty nanosecond length pulses were reflected off a diffuse white screen into an 8-inch diameter Celestron telescope. A silicon avalanche photodiode was used as a detector. The received signal was well within limits for further design analysis.

Design and construction of the prototype test model, with closer adherence to the objectives listed above, was already underway when this thesis work began.

II. SYSTEM ANALYSIS

Operation of the laser altimeter is similar to other rangefinders. The output signal level from the detector can be determined by tracing the light pulse through each step of its travel and taking into account all gains and losses. This will lead to a trade-off equation. Improving gains and reducing losses can then be weighed against the objectives listed in Chapter I. Limitations due to physical constraints also become apparent. Figure 1 shows the path of a typical signal pulse used for the analysis. Steps 1 through 5 determine the signal voltage of the detector.

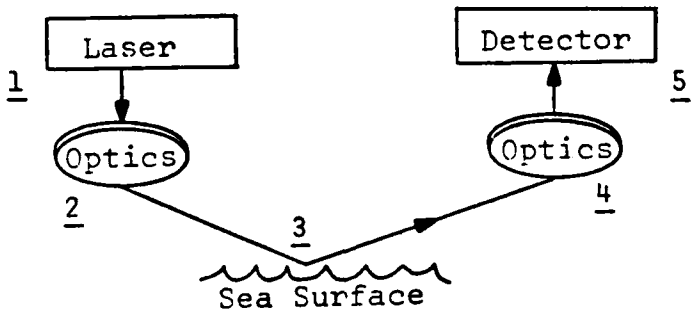

Fig. 1 Path of a Light Pulse

A. THE TRADE-OFF EQUATION

The following list of variables will be used in the derivation.

P_t = transmitter peak power

E_r = energy received at the detector

τ = transmitter pulse length

Ω_t = solid angle of the transmitted beam

h = height of the altimeter

T_t = transmission factor from power source to target

T_r = transmission factor from target to detector

r = reflectance of sea water

R_f = reflection factor for the sea surface

A_e = effective receiver aperture area

D = aperture diameter

f = focal length of the receiver optics

f/# = ratio of focal length to aperture diameter

Ω_{fov} = solid angle of the receiver field-of-view

A_d = area of the detector

R_s = responsivity of the detector

C = capacitance of the detector

V_s = signal voltage at the detector output

The light pulse starts from a laser source. The energy contained in a single pulse is $P_t \tau$ (Step 1). It is sent through the output optics to form a beam of solid angle Ω_t. This also causes a reduction in energy due to reflection at

each lens surface. Losses due to atmospheric absorption and scattering also occur so that by the time the pulse reaches the sea surface it has energy per steradian of $P_t \tau T_t / \Omega_t$. (Step 2)

The sea surface is a distance h away. The energy spreads as the square of the distance so the energy per unit area striking the surface is $P_t \tau T_t / \Omega_t h^2$.

Reflection at the sea surface causes loss in two ways. Light incident on an air-water interface undergoes transmission and reflection. At normal incidence, the amount reflected is determined by the index of refraction, n, of the water. The Fresnel reflectance coefficient is

$$r = \left[\frac{n-1}{n+1}\right]^2 \quad .$$

This is the fraction of energy reflected.

The second loss is due to the geometry of the reflection. Energy can be reflected anywhere in the hemisphere above the sea surface. The amount reflected back toward the receiver aperture depends on the roughness of the surface, the transmitter beam angle of incidence, and the beam pattern. The reflection factor, R_f, indicates how much energy reflects from a unit area of the sea surface into a unit area at the aperture. See Chapter III for further discussion. (Step 3)

The effective aperture area, A_e, is a measure of the light gathering power of the receiver. It accounts for the actual aperture size and transmission losses between the sea surface and the detector.

Multiplying by the last three factors gives the total energy received at the detector,

$$E_r = \frac{P_t \tau T_t r R_f A_e}{\Omega_t h^2} . \qquad \text{(Step 4)}$$

A detector with responsivity R_s [amps/watt = coul/joule] will convert the energy of the light pulse, E_r, into a charge $Q = E_r R_s$. The detector acts as a capacitor to store the charge which increases its voltage an amount $V_s = Q / C$. Therefore, the signal voltage at the detector output is

$$V_s = \frac{P_t \tau T_t r R_f A_e R_s}{\Omega_t h^2 C} . \qquad \text{(Step 5)}$$

This is the trade-off equation; however, some algebraic manipulation will make it more useful.

The effective aperture area can be replaced by the actual area, $\pi D^2 / 4$, times the transmission loss factor T_r. With $f/\# = f / D$ and the receiver field-of-view $\Omega_{fov} = A_d / f^2$, the equation becomes

$$V_s = \left(P_t \tau T_t \right) \left(\frac{r R_f}{\Omega_t h^2} \right) \left(\frac{\pi/4 \; T_r}{(f/\#)^2 \; \Omega_t} \right) \left(\frac{A_d R_s}{C} \right)$$

The four terms of this equation correspond to the design areas of the transmitter, reflection, receiver, and detector, respectively. The transmitter beam solid angle has been included with the reflection term because R_f is closely dependent on it. The design parameters related to the transmitter, receiver, and detector terms are discussed below. The reflection term is reserved for Chapter III.

1. Transmitter

Lasers provide a nearly ideal power source for rangefinders. Several types are available to choose from; He-Ne, CO_2, Ruby, Nd:YAG, and GaAs are all used in current systems. Gallium Arsenide laser diodes have many advantages. They are small, inexpensive, and shock resistant. They operate in the infra red at a wavelength of 904 nm.

Although stacked arrays can reach peak powers of 1200 watts, cost becomes excessive for peak powers above about 100 watts. Power supply requirements (less than 100 V) can be supplied by battery.

Modulation of the output is easily achieved by electronics. Commercially available pulsers were used for this stage of development but further designs will require a

separate pulser design and integration of electronics into a single package which should reduce the size and cost.

The transmitter term shows the signal voltage directly proportional to the energy of the pulse, $P_t\tau$. Higher power or a longer pulse would increase the energy. The limit of the pulse length is usually determined by the heat that builds up within the laser diode when it operates. A typical maximum pulse length at maximum power is about 200 nsec [Ref. 6]. Longer pulses can be used but only at reduced power so that the energy of the pulse would be about the same.

The maximum pulse repetition frequency (PRF) is determined by the duty factor, typically .02%, by the formula PRF = Duty Factor / τ, or 1 kHz for the values given. Shorter pulses allow higher PRF's, but measurements at one thousand times per second is more than adequate here. Detector characteristics also affect PRF and will be considered later.

Pulse length should be much less than the round trip travel time to the target. At 150 meters, the round trip equates to 1.0 μsec. A τ of 200 nsec should yield only fair precision. The objectives stated in Chapter I do not require a highly precise measurement, but a shorter pulse length may be necessary. In general, a higher power/short pulse is better than a low power/long pulse of the same energy.

T_t is the last transmitter factor. It includes the transmittance of the output optics and atmospheric propagation to the sea surface. The laser diode has a natural beam pattern of about 8^o x 24^o. Each lens used to produce the desired pattern will cause about a 8% loss of energy. This is determined by the Fresnel reflection coefficient described above but for the air-lens interface. An outer protective nose dome must be used at the cost of another 8%.

Atmospheric absorption and scattering losses must also be considered. High resolution transmittance data published by McClatchey and Selby [Ref. 7] show neglible absorption at 904 nm wavelength. Scattering losses are also shown to be negligible in a clear atmosphere (visibility > 23 km). However, when clouds, rain, or fog are present, the scattering loss can be essentially complete [Ref. 8]. The transmittance under these conditions depends on the water droplet concentration and size distribution. This may prove to be a major limitation in the system operation.

2. Receiver

The receiver focuses the incoming light onto the surface of the detector. A filter is included to reduce unwanted background radiation.

The aperture diameter limits the total amount of power received. It should be large to receive the most power, but

one objective is that the system be small. Three designs are shown in Figure 2. Designs a) and b) have the same size aperture and detector. However, design a) has an f/# three times that of b) so that the field-of-view of b) is nine times that of a). Therefore, b) can focus much more signal onto the detector. In general, a smaller f/# increases the intensity of the return signal incident on the detector.

Designs b) and c) have the same f/# so, that although b) gathers more light than c), the intensity on the detector is the same. When capacitance of the detector is taken into account, the signal voltage is shown to depend on the intensity rather than power on the detector. Therefore, the actual size of the aperture can be scaled larger or smaller without loss of signal. See the next section for further discussion.

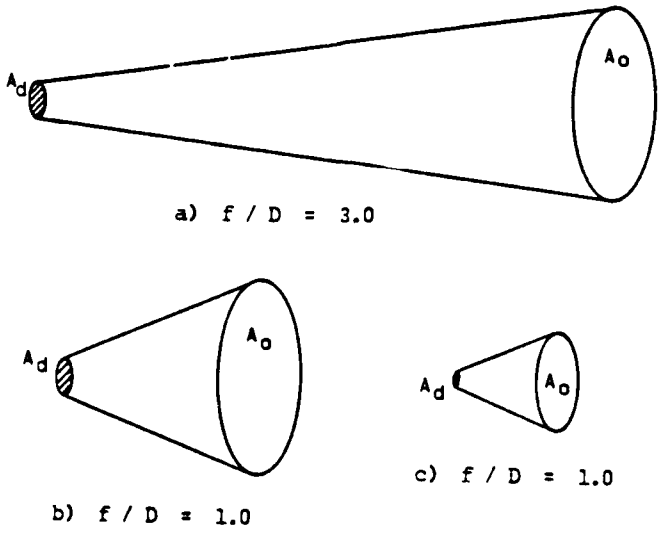

Fig. 2 Receiver Optics Geometry

Although smaller is generally better, the receiver need not be tiny. Ease of construction, alignment of the field-of-view, and parts availability set a practical limit.

The f/# is determined by the focusing lens. Fresnel lenses can provide f/#'s as low as 1.0 and have several advantages over conventional lenses. Figure 3 shows a diagram of each. With the bulk removed, the Fresnel lens's lower mass and thin disc shape make it easier to work with and less susceptible to fracture. They are produced with aspheric curvature to reduce aberrations. A single lens focusing system is preferable to reduce reflection losses but will depend on the detector geometry and beam pattern.

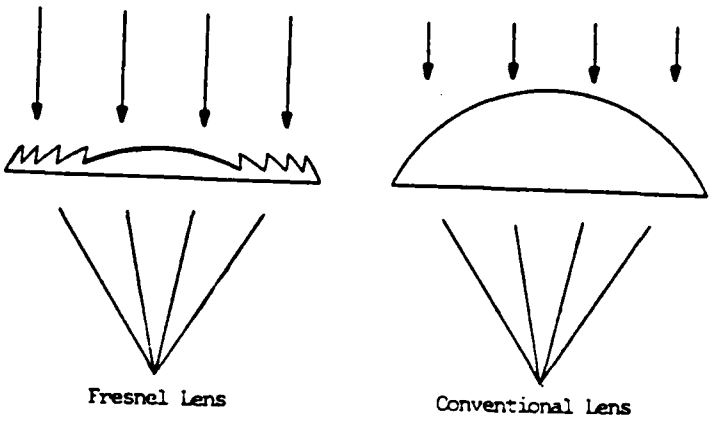

Fig. 3 Lens Type Comparison

The field-of-view should be small according to the trade-off equation. If it is smaller than the transmitter beam pattern, however, some of the return signal entering the aperture will be missed. A field-of-view which exactly matched the transmitter beam would be ideal but a slight enlargement may be necessary to allow for alignment errors. The field-of-view is determined by the focal length of the lens and the detector size and geometry.

A narrow bandpass filter placed in front of the detector will reduce the background light considerably. High quality interference filters for infra-red wavelengths are commercially available with bandwidths as narrow as 10 nm. They are not cheap and are limited in size to about 2 inches in diameter.

The line width of the laser diode selected for use is 3.5 nm (Full Width at Half Maximum) which fits well inside the 10 nm band. This is true for light at normal incidence to the filter surface. Reference 9 shows that a 30° angle of incidence decreases the center wavelength of the filter by more than 1% . For λ = 904 nm, this equates to about a 9 nm shift. Much of the signal would then be outside the bandpass. The solution is either to limit the angle of incidence or widen the band limits.

Figure 4 shows two placement schemes for the lens filter combination. The first allows for an aperture area larger than the filter but, as can be seen, a significant

portion of the incoming light strikes the filter at high angles of incidence. A wider bandwidth would be required to pass the light and would therefore cause higher background

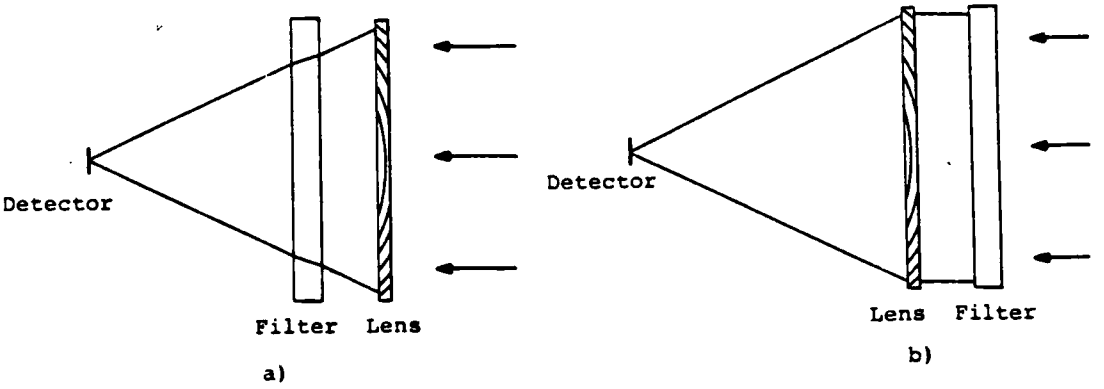

Fig. 4 Lens/Filter Configurations

noise levels. Placing the filter in front of the lens as shown in b) limits the angle of incidence to the maximum of the field of view. A 10^{o} angle causes a shift of about .2% or less than 2 nm which is well within the 10 nm bandwidth. The aperture size is then limited to the size of the filter (2-inch diameter).

The transmission factor, T_r, is similar to T_t. The losses due to the lenses, nose dome, and atmospheric propagation are the same. The filter causes an additional loss factor of about 50% .

3. Detector

The detector converts infra-red radiation into an electrical signal. There is a wide variety of available types with photo-multiplier tubes, avalanche photodiodes, and P-I-N photodiodes being most common for rangefinding systems. The characteristics of the P-I N photodiode best match the listed objectives. They are small, shock resistant, relatively inexpensive, and they operate on less than 100 V power supply. The most significant disadvantage is that responsivity is limited to about 0.5 amps/watt.

The P-I-N detector circuit is shown in Figure 5. A reverse bias voltage is applied so that it operates in the "photoconductive" mode. The capacitance of the detector results in a pulsed light signal being integrated to produce a change in voltage of $V_s = R_s E_r / C$. Figure 6 shows the rise in voltage proportional to the length of the pulse. For this mode, the decay time of the detector must be long compared to the rise time.

The total power incident on the detector is the sum of the background noise and the signal pulse. If the background signal is too large, the detector will saturate; that is, the change in voltage due to the dc signal will equal the bias voltage. The detector will then be in a photovoltaic mode which is undesirable. The solution is to keep the interference filter bandpass as narrow as possible

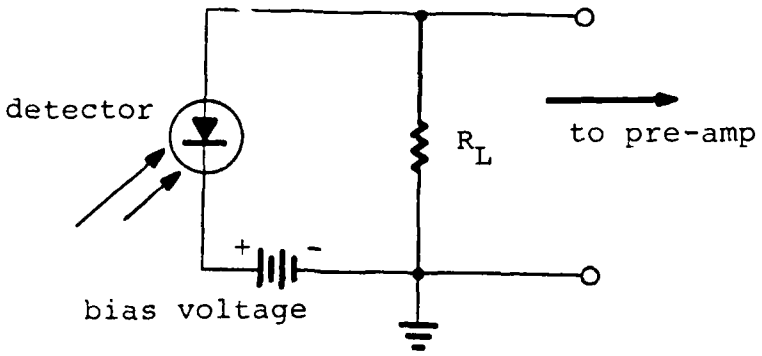

Fig. 5 Detector Circuit

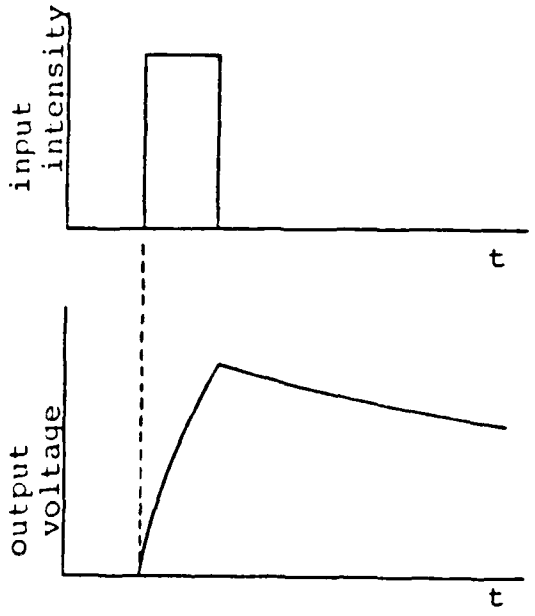

Fig. 6 Detector Response

to reduce the background signal and then increase the bias voltage well above the saturation level.

A high bias voltage (~50V) will reduce the detector capacitance and also decrease the rise time. The benefit of reduced capacitance can be seen from the trade-off equation where it shows directly the increase in V_s. Maximum PRF also depends on the capacitance. The decay time of the detector, τ_d, is equal to $R_L C$. If the time between pulses is insufficient for complete decay of the signal, the level will build up over several pulses and yield an incorrect altitude.

The rise time determines how quickly the voltage changes when a light pulse strikes the detector. A higher bias results in a faster rise time. This is due to the mobility of the free charge carriers produced in the semiconductive layer. Faster rise time improves the timing accuracy of the system. The leading edge of the signal voltage determines its "arrival" time. Noise which adds or subtracts from the leading edge will advance or retard the arrival time to produce an error in the attitude measurement. A signal which rises quickly has less room for error.

Performance data for a silicon photodiode detector is given in Figure 7 [Ref. 3]. Responsivity is near optimum for the 904 nm wavelength. Rise times can be as low as a few nanoseconds. The capacitance of a P I N detector is

Si

T_d = 300 K
A_d = wide range
R_d = 50 to 5 kilohms
τ = 2×10^{-7} sec
$\mathcal{R}_{\lambda_p}$ = 650 mA W^{-1}

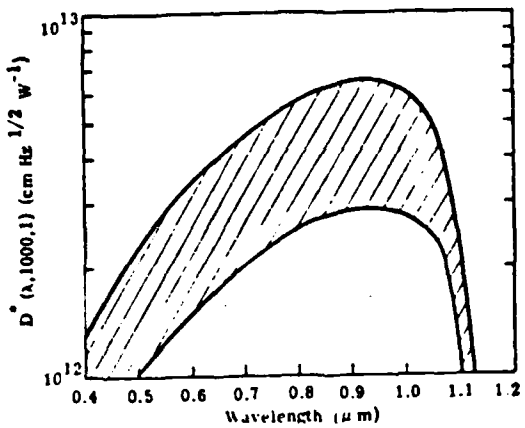

(*a*) Spectral response of detector D* (λ, 1000, 1).

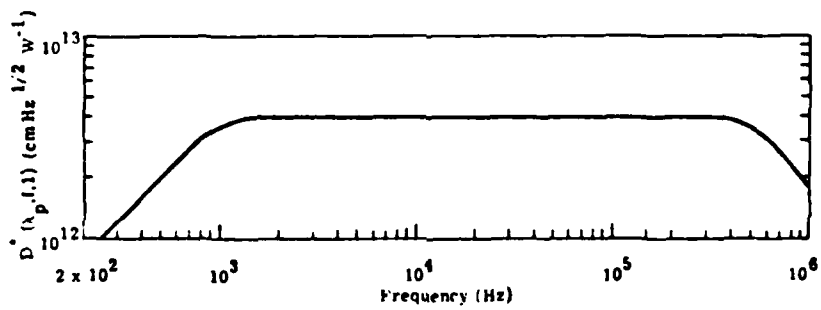

(*b*) Frequency response of detector D* (λ_p, *f*, 1).

Note

(1) Small detectors have been made in arrays on 0.6 mm centers or less, and large detectors several centimeters in diameter or more have been made.

(2) $\mathcal{R}$ depends upon bias voltage.

(3) Capacitance can vary from 2 to 800 pF, depending on bias.

Fig. 7 Si detector performance data at 300 K. [Ref. 3]

proportional to its area. Therefore, a large area, large capacitance is no better or worse than a small area, small detector. This can be seen from the trade-off equation. For the terms which affect the size of the system,

$$V_s \propto \frac{A_d}{(f/\#)^2\, \Omega_{fov}\, C} = \frac{A_d}{\frac{f^2}{D^2} \cdot \frac{A_d}{f^2}\, C} = \frac{D^2}{C} = \text{constant!}$$

This is a constant since $D^2 \propto A_o$ and $C \propto A_d$. Figure 2 shows two sizes, b) and c), which yield the same signal voltage since the f/# and Ω_{fov} are the same in both cases. Thus, the entire system can be scaled up or down in size (within practical limits) without loss of signal voltage.

The signal voltage can be found with the above analysis but the signal-to noise ratio is the actual parameter used to determine how well the system works. Sources of noise include background radiation, detector leakage current, thermal noise, and quantum noise. Background radiation, consisting primarily of scattered and reflected solar light, is the major source of noise.

Ross [Ref. 10] delineates the conditions for minimizing background noise when it is the limiting factor. The bandpass filter should be as narrow as possible, the field of view should be as small as possible, and the post detection bandwidth should be the minimum that will pass the

information. The first two conditions have been met through use of the trade-off equation. The last is a function of the pre-amp and amplifier design and is discussed below. Thermal (Johnson) noise is the second major source of noise. The mean square thermal noise voltage is given by

$$V_n^2 = 4\ k\ T\ B\ R_L$$

where k = Boltzman's constant
T = Temperature
R_L = Load resistance
B = System bandwidth

Thus, the system bandwidth should be small to reduce thermal noise as well. This value is a lower limit for the total noise of the system. R_L conforms to the detector and bias voltage parameters to prevent saturation and the bandwidth should already be reduced to a minimum. The only factor left is the temperature. A cooling system would be needed to reduce it but is not considered feasible within the size and cost objectives.

B. THE SYSTEM

A complete block diagram of the system is shown in Figure 8. A timing sequence starts with a pulse at step 1 which signals the transmitter to fire. A short burst of infra-red energy is sent toward the target at step 2. Reflected energy is received and converted into an electronic signal at step 3. The signal is amplified and

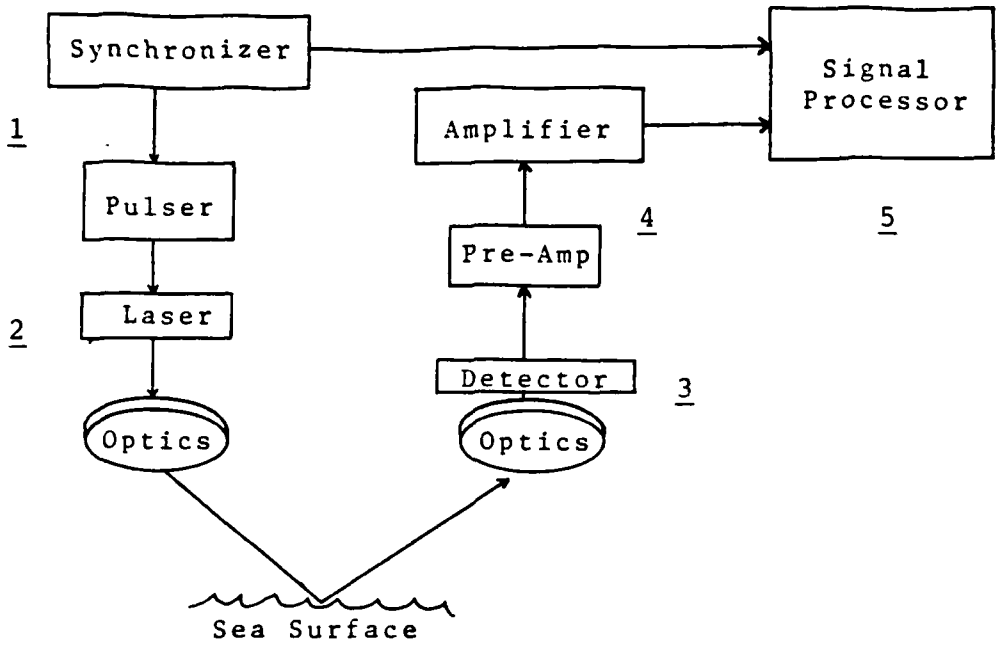

Fig. 8 System Block Diagram

sent to the processor at step 4. If the signal is received within the set time delay, an output signal is sent at step 5.

A brief description of the electronic components is given below; however, detailed discussion of the electronics is beyond the scope of this thesis. Figure 9 shows a typical signal for each component. Figure 10 shows four possible situations within the signal processor.

The synchronizer provides timing pulses for the entire system. Oscillation pulses are produced by an integrated circuit with a variable frequency adjustment. A frequency in the kilohertz range will provide near-continuous

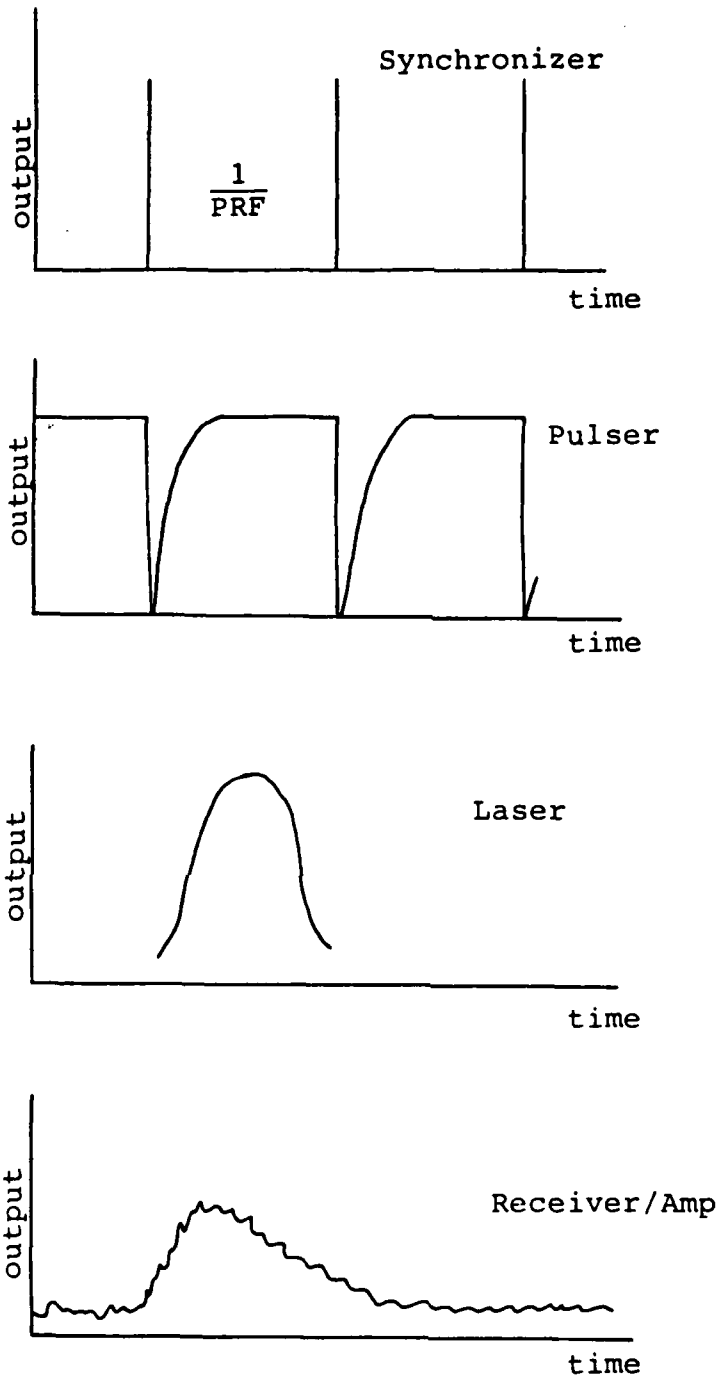

Fig. 9 Typical Component Signals

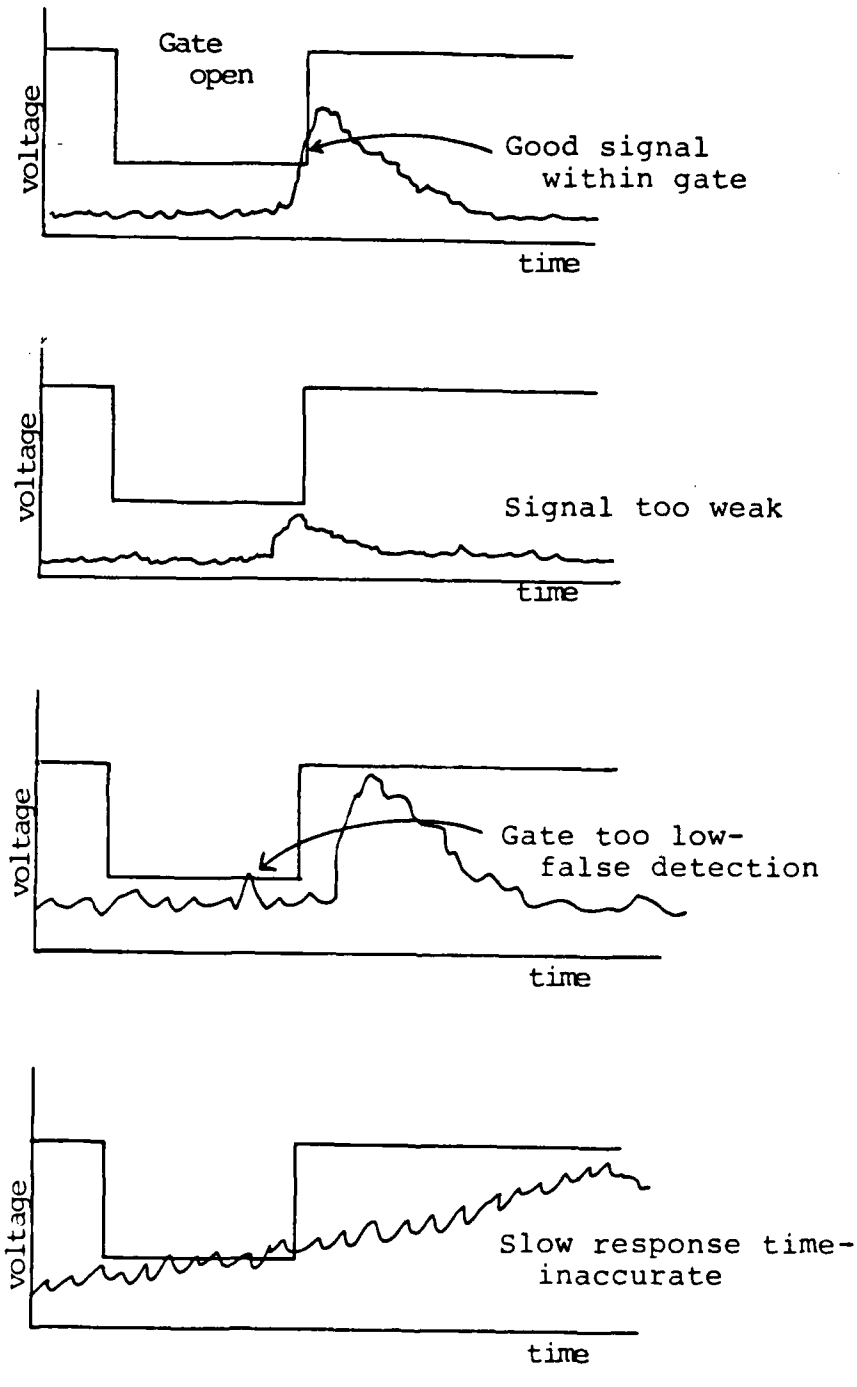

Fig. 10 Signal Processing

operation with a duty cycle sustainable by the laser diode. The detector recovery time is also short enough to prevent pulse-to-pulse build up. The laser pulser stores energy between pulses and releases it when a timing pulse is received. A silicon controlled rectifier allows a short burst of high current to be sent to the laser. The pulse width and pulse shape are determined by the pulser and laser diode characteristics.

The pre-amplifier converts the detector output into a signal suitable for amplification. A capacitor decouples the modulated signal from the dc component and sends it to a pre-amp transistor. A JFET is used in an emitter-follower configuration. The bandwidth should be kept to a minimum to reduce the effect of background noise. To pass the signal effectively, however, it will need to be on the order of $1/2\pi\tau$ or about 2 MHz for a 100 nsec pulse.

A single video amplifier can boost the signal enough to be processed. A comparator in the signal processor starts a gate with the initial sequencing pulse. An output signal is sent if the received pulse is detected within the gate. Minimum signal level can be adjusted to reduce the probability of false detection. The gate width determines the activation altitude and is also adjustable. A counter may be necessary to improve precision.

Power supply requirements range from 5 to 80 volts. Batteries can be kept small since operation is limited to

about two minutes. Shielding is a necessary part of the design to prevent crossover signals.

A last part of the design is the container which includes a nose dome for aerodynamic efficiency. It must be transparent in the infra-red and its curvature must be considered in transmitter and receiver optics. Construction must be tough enough to withstand high g-forces.

Development of the laser altimeter system involves two distinct phases. The theoretical stage determines the parameters to be considered and how they interrelate. A trade-off equation is an effective way to gain understanding as to just what's needed in the system. The experimental stage determines the limits of the trade-off equation. Realistic, engineering trade-offs must be made. Construction of a component often leads to changes in design. Only by continual analysis and testing will a working system result.

III. SEA SURFACE REFLECTION

The reflection factor, R_f, indicates how much of the light that is reflected from the sea surface returns toward the receiver aperture. It will depend on the transmitter beam pattern, the attitude of the transmitter (which determines the angle of incidence), and the sea state. Each of these effects must be considered when applying the reflectivity to the trade-off equation.

Reflection of light can be either specular or diffuse. Most surfaces will exhibit both, but one is usually dominant. Specular reflection is that of a mirror surface where the reflection angle equals the incident angle. For low sea states this will dominate. Diffuse reflection occurs when the power reflected varies over all angles. This will dominate for high sea states (whitecaps).

A. SPECULAR REFLECTION

At low sea states, the surface of the water can be considered as a collection of wave facets. That is, small flat areas inclined at various angles. A ray of light which strikes the sea surface will reflect in a direction depending on the direction of the wave facet inclination. Figure 11 shows a one-dimensional view. The inclination of each facet changes with time due to wave motion. For light

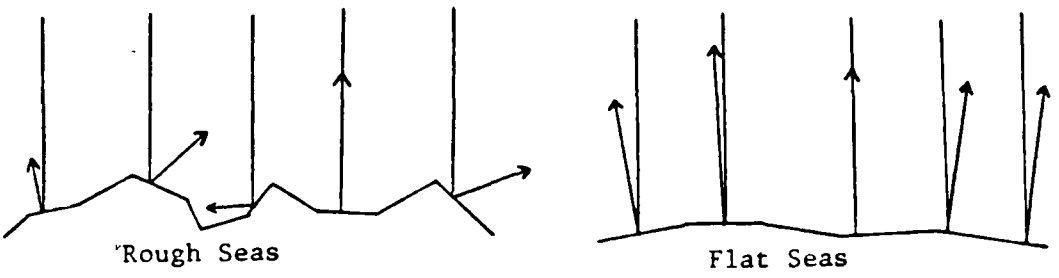

Fig. 11 Wave Facets of the Sea Surface

wind conditions, the sea is "flat". The normal of a wave facet does not vary much from vertical. During high sea states, the normal of a wave facet is rarely vertical and often tilted at large angles.

Cox and Munk [Ref. 11] determined the probability distribution function for the wave slope angles as a function of wind velocity. This distribution can be used to calculate the reflection factor, R_f.

A single light ray which strikes the ocean surface has a certain probability of hitting a wave facet that is at just the right inclination to reflect back into the receiver aperture. The tolerance in the inclination angle depends on the solid angle spanned by the aperture. A large aperture close to the surface will receive reflected rays over a wide range of wave facet inclinations. A small aperture far from

the surface will require the wave facet to be within a very narrow range of inclinations.

A divergent transmitter beam will have light rays which span a given solid angle. The direction angles of each light ray determine its probability of reflection back into the aperture (equal to the probability that the wave slope is within tolerance). Integration over all direction angles within the beam solid angle yields a probability of back reflection for the entire beam. For a beam which spreads over many facets, the probability becomes a percentage of reflected power which enters the receiver aperture; i.e., R_f.

The inclination of a wave facet requires two angles to be defined. Let α and β be such that

α = the angle clockwise from the wind direction (y-axis) to the vertical plane containing the line of steepest ascent of the wave facet.

β = the angle from vertical to the normal of the wave facet. (Figure 12)

The direction angles of a light ray emitted by the transmitter can be specified by similar angles α' and β' (Figure 13).

Power is reflected back toward the aperture only if $\alpha = \alpha'$ and $\beta = \beta'$ within the limits spanned by the size of the aperture. The probability that a wave slope is within $\alpha \pm d\alpha/2$ and $\beta \pm d\beta/2$ is given by Cox and Munk as

$$p(\alpha,\beta)\ \tan(\beta)\ \sec^2(\beta)\ d\alpha\ d\beta\ .$$

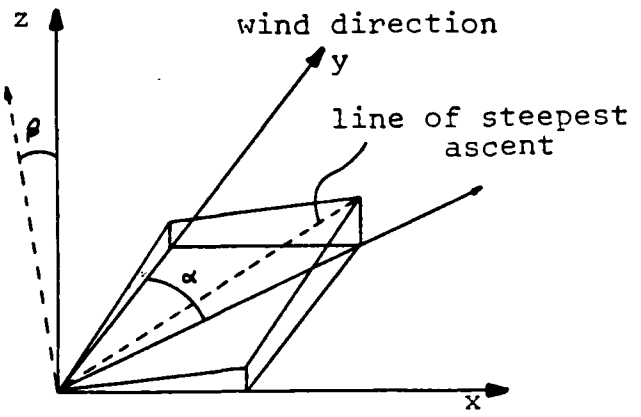

Fig. 12 Wave Facet Angles

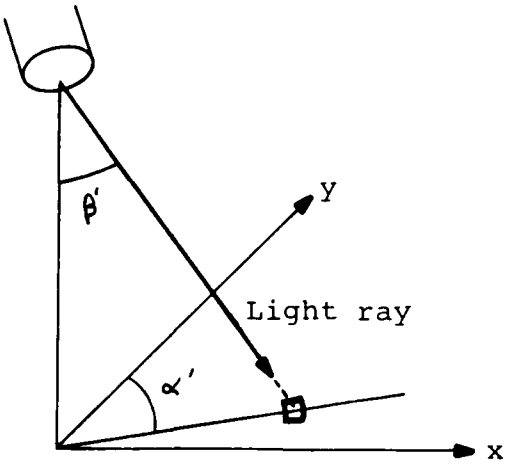

Fig. 13 Light Ray Angles

The function $p(\alpha,\beta)$ is a two dimensional Gaussian multiplied by a Hermite polynomial which corrects for wind effects.

A wave facet spans a differential solid angle $d\Omega_t$ within the transmitter beam pattern. For a total transmitter power, P_t, spread over a beam divergence angle, Ω_t, the power incident on a wave facet is

$$dP_t = \frac{P_t \, d\Omega_t}{\Omega_t} .$$

The Fresnel reflectance coefficient determines how much of that power is reflected (vice transmitted or absorbed). The probability distribution determines the average power distribution of back reflection. Therefore, the average

differential power received at the aperture within $\alpha \pm d\alpha/2$ and $\beta \pm d\beta/2$ from a wave facet is

$$d^2P_r = \frac{P_t \, d\Omega_t \, r \, p(\alpha,\beta) \, \tan(\beta) \, \sec^2(\beta) \, d\alpha \, d\beta}{\Omega_t} .$$

This can be integrated over the entire transmitted solid angle to give the power reflected from all wave facets into differential angles $d\alpha$ and $d\beta$ at the receiver. Integrating over the solid angle subtended by the receiver aperture, Ω_r, gives, P_r, the total power received.

Thus,

$$P_r = \iint_{\Omega_r} \iint_{\Omega_t} \frac{P_t \, d\Omega_t \, r \, p(\alpha,\beta) \, \tan(\beta) \, \sec^2(\beta) \, d\alpha \, d\beta}{\Omega_t} \quad \text{(EQ. 1)}$$

Some simplification of EQ. 1 is in order. Figure 14 shows a typical wave facet within the beam pattern determined by direction angles α and β. The entire transmitter beam is tilted to the directions α_o and β_o because of the altimeter swing. Define θ to be the angle from the center of the beam axis to the direction of the wave facet and ℓ to be the slant distance from the aperture to the wave facet.

Then the differential solid angle spanned by a differential area of the aperture from the wave facet is

$$d\Omega_r = \frac{dA \cos(\theta)}{\ell^2} .$$

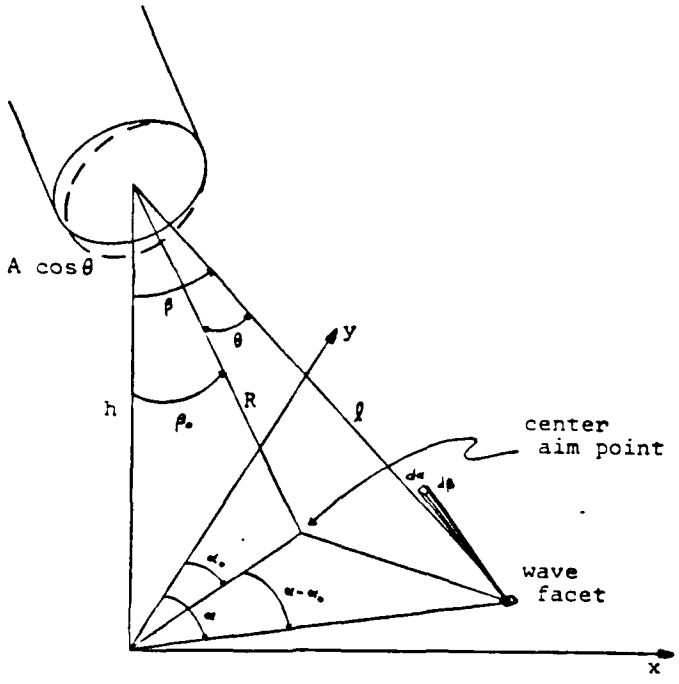

Fig. 14 Wave Facet/Beam Pattern Geometry

But, $d\Omega_r = \sin(\beta)\, d\alpha\, d\beta$

and $\ell = h / \cos(\beta)$.

Combining yields $\tan(\beta) \sec(\beta)\, d\alpha\, d\beta = \dfrac{dA \cos(\theta)}{h^2}$.

Substituting into EQ. 1 yields

$$P_r = \iint_A \iint_{\Omega_t} \frac{P_t\, d\Omega_t\, r\, p(\alpha,\beta) \sec(\beta) \cos(\theta)\, dA}{\Omega_t\, h^2}.$$

The integral over the solid angle subtended by the aperture has been converted to an integral over the aperture area. The terms P_t, r, Ω_t, and n are all constant and can come outside the integrals. The aperture area is small compared

to the distance h so the angles α and β can be considered constant for the integration over A. Therefore, the power received becomes

$$P_r = \frac{P_t\, r}{h^2\, \Omega_t} \iint_{\Omega_t} p(\alpha,\beta)\, \sec(\beta)\, \cos(\theta)\, d\Omega_t \iint_A dA$$

or,

$$P_r = \frac{P_t\, r\, A}{\Omega_t\, h^2} R_f \qquad \text{(EQ. 2)}$$

where $R_f = \iint_{\Omega_t} p(\alpha,\beta)\, \sec(\beta)\, \cos(\theta)\, d\Omega_t$ is the reflection factor given in the trade-off equation.

This equation for R_f was evaluated by the author. The IMSL subroutine DBLIN [Ref. 12] was used for the two-dimensional integration. Three transmitter beam patterns were used for Ω_t; Ω_1 is a 1^o x 1^o pencil beam, Ω_2 is a 1^o x 10^o offset fan-shaped beam, and Ω_3 is a 20^o x 20^o wide angle beam (See Figure 15). Variation with angle of incidence was determined from zero to ten degrees at a wind speed of 5 m/s. Variation with sea state was determined for windspeeds up to 14 m/s at two angles of incidence, zero and nine degrees.

The results are plotted in Figures 16 and 17. The curves shown are of R_f/Ω_t, the reflection factor per transmitter beam solid angle. This is a more useful

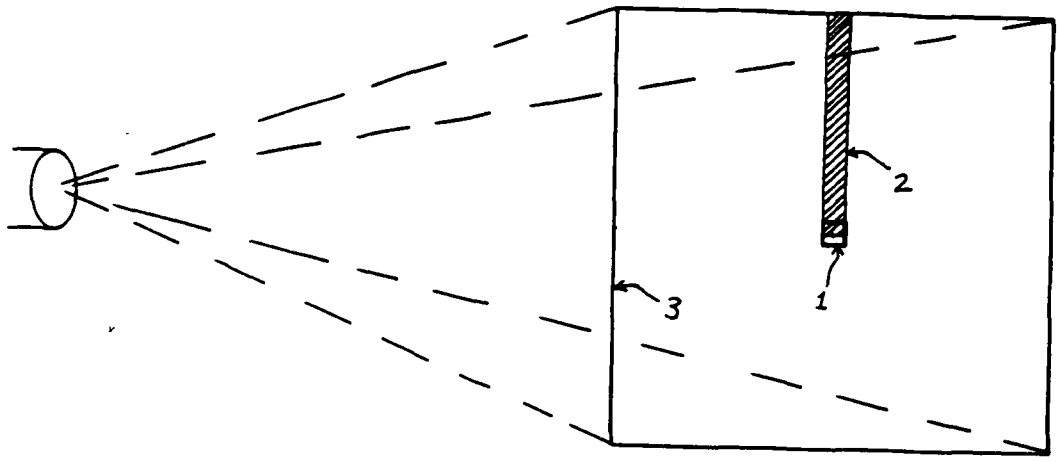

Fig. 15 Beam Patterns

parameter to compare because it normalizes R_f to a constant transmitter power. That is, pattern Ω_2 covers ten times the area of pattern Ω_1 but pattern Ω_1 has ten times the power density. R_f/Ω_t takes this into account.

The offset fan-shaped beam is not symmetric and therefore the angle of incidence depends on the orientation of the beam. Figure 18 shows the two limiting cases for a 10^o angle. The tilt can move the pattern away from normal (Ω_{2-}) or toward normal incidence (Ω_{2+}), or at some sideways direction which will give a value between the two limits.

The results show behavior as would be expected. Figure 16 shows that a narrow beamwidth at normal incidence yields a greater R_f/Ω_t value, especially at low wind speeds. For

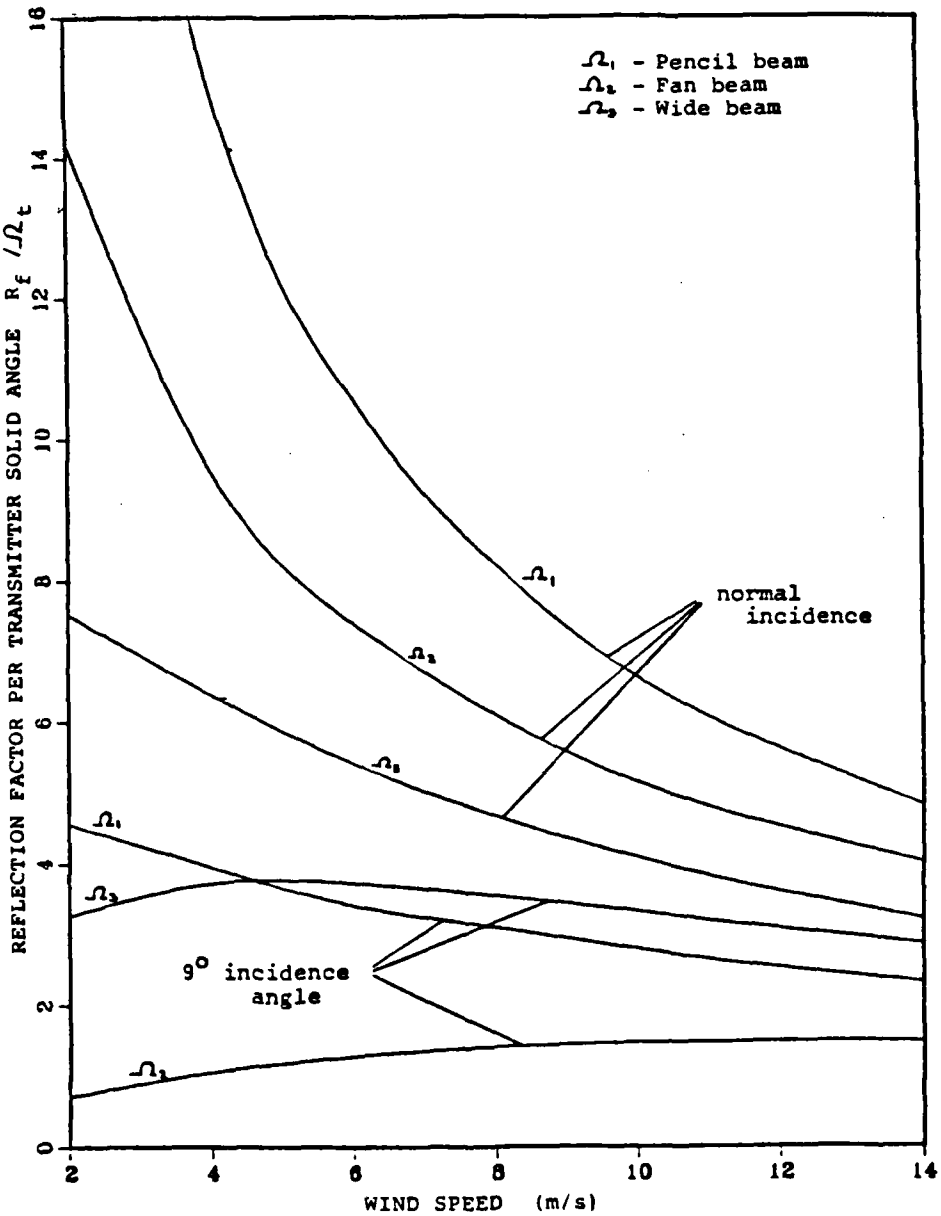

Fig. 16 R_f/Ω_t vs. Wind Speed at normal and 9^o incidence.

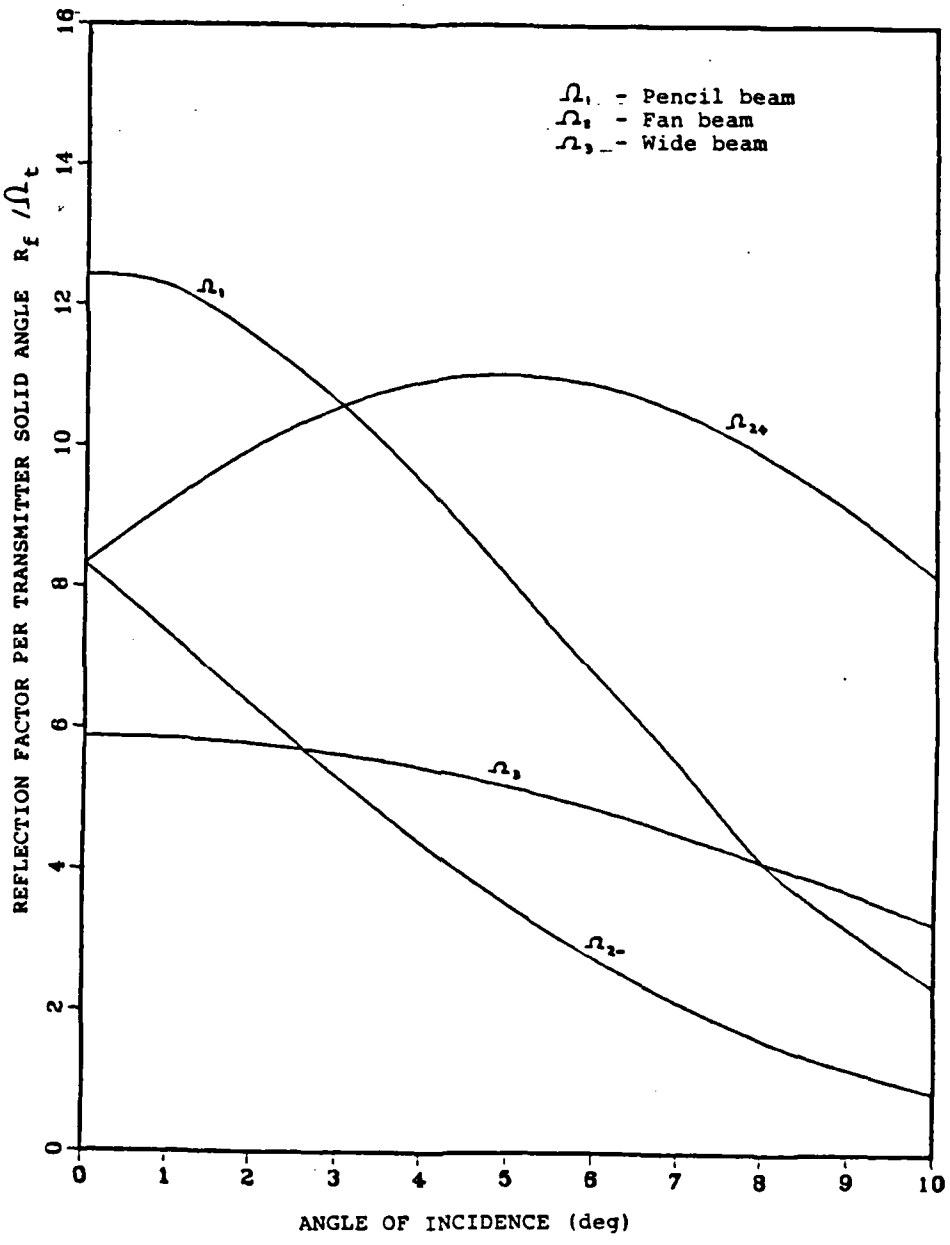

Fig. 17 R_f/Ω_t vs Angle of Incidence.

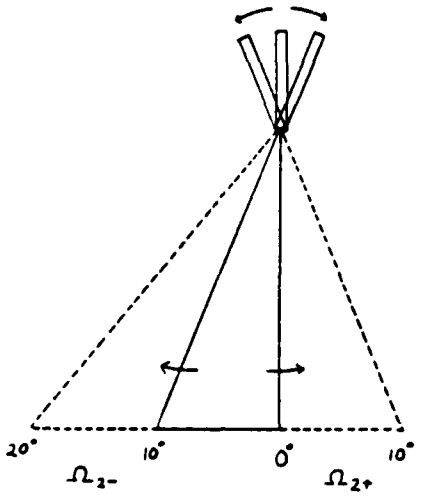

Fig. 18 Offset Beam - 10^{o} Angle of Incidence

an altimeter inclination of 9^{o}, the values are much lower; most significantly for the narrow beamwidth and only slightly for the wide angle beamwidth.

The effect of angle of incidence is reduced for high sea states. Many more wave facets become inclined at large angles. This causes back reflection contributions to be more evenly distributed over the entire beam pattern.

Figure 17 shows the dependence on angle of incidence more clearly. The pencil beam starts with the highest value and falls off dramatically at increasing angles. The wide angle beam pattern starts the lowest but decreases very little. The Ω_{2} curve for the fan-shaped beam tilting away from normal incidence becomes substantially less than the Ω_{2} curve at 10^{o}.

Conclusions are that 1) the wide angle pattern yields the most consistent but generally the lowest value of R_f/Ω_t, 2) the pencil beam pattern yields the highest value but is most susceptible to angle of incidence, and 3) the fan shaped beam can yield a value quite high or quite low depending on the orientation.

Significance can be found in the Ω_{2+}/Ω_2 curves through the dynamics of the altimeter. Operation is assumed to occur during a parachute retarded descent which causes the altimeter to oscillate as a two-dimensional pendulum. For a characteristic length L, equal to the distance from the parachute center of effort to the center of mass of the payload, the period of oscillation is about $T = 2\pi\sqrt{L/g}$ where $g = 9.8$ m/sec^2. Then, for an assumed $L \approx 2$ m, $T = 2.8$ sec.

The altimeter will swing in an elliptical pattern such that the orientation of the fan beam will cycle every 2.8 seconds. This is the maximum time between conditions for which the R_f/Ω_{2+} curve would apply. If this condition is required to yield a signal strong enough for detection, then the maximum error in the altitude would be 2.8 sec x descent rate. The descent rate specified is about 10 m/s for a maximum error of 28 meters. This is a worst case error. Intermediate values approach the maximum smoothly until a strong enough signal is detected.

This analysis also applies for the pencil beam pattern. The angle of incidence swings through a minimum which is not necessarily zero degrees. Nearly circular swings could be set up such that the angle stayed about 10^{o}, but this should be rare. Figure 17 shows that for a 5 m/s windspeed, the angle need only decrease to 3^{o} to beat the value of R_f/Ω_{2+}. A closer study of the specific vehicle dynamics is needed for further analysis.

Measurements of sea surface reflectivity at .9 μm were reported by Stephens [Ref. 13] for predominantly specular reflection. Conical beam patterns of 2, 4, 8, and 16 degree beamwidths and fan-shaped beams of $2^{o} \times 8^{o}$ and $2^{o} \times 16^{o}$ were used from a height of 25 feet above the water surface. Angle of incidence was varied from zero to 20^{o}. Wind speeds ranged from 3.5 to 13.0 knots. Reflectivity values reported were normalized to a 100% effective diffuse reflector.

One conclusion drawn by Stephens was that for a constant power transmitter, beam size had only a slight effect of reflectivity. A 64-fold increase in the beam solid angle decreased the reflectivity by a factor of less than 2. Figure 16 shows similar behavior of R_f/Ω_t for a 400-fold increase in beam size.

Figures 16 and 17 show values consistent with those measured. Figure 19 shows measured data for a 2 degree beamwidth. Data for the $1^{o} \times 1^{o}$ beam taken from Figures 16 and 17 has been added and agrees quite well. Variations due

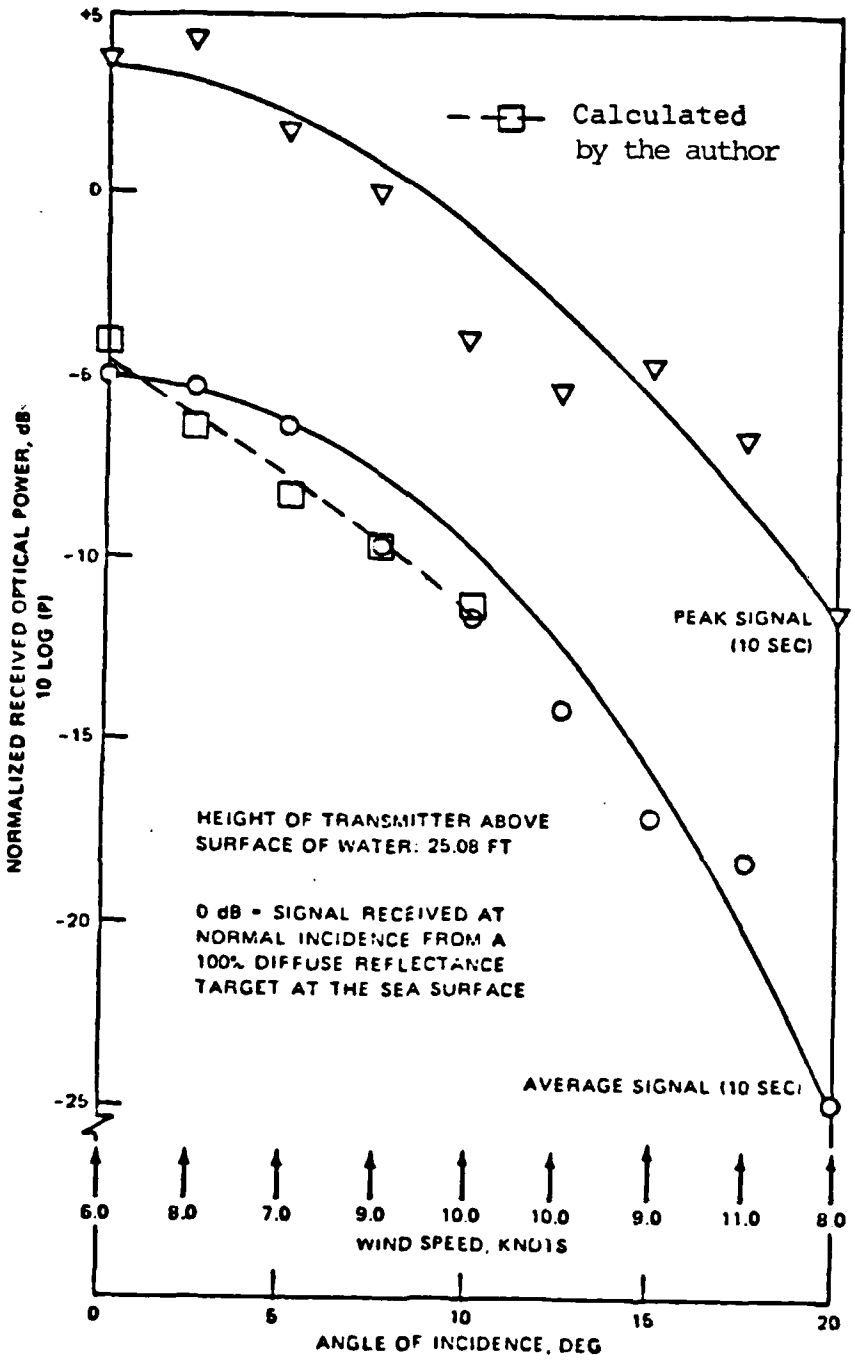

Reflectance Characteristics of the Sea Surface for a 2-Degree Transmitter Beamwidth.

Fig. 19

to changes in windspeed can be significant for speeds less than 10 knots and account for some of the differences.

Another conclusion by Stephens is that the wider beamwidths yield smoother, less rapid fluctuations. Raw reflectance data shown in Figure 20 indicates peak values occur about once every 2 seconds for the 16 degree beamwidth. This corresponds to a spot size on the sea surface of 25 tan(16^{o}) ≈ 7 feet in diameter. A 1^{o} spot at 150 m is about 9 feet in diameter. Thus, the fluctuations should be nearly equivalent, ignoring angle of incidence variations. At the higher altitude, the wider beam patterns would produce essentially constant returns.

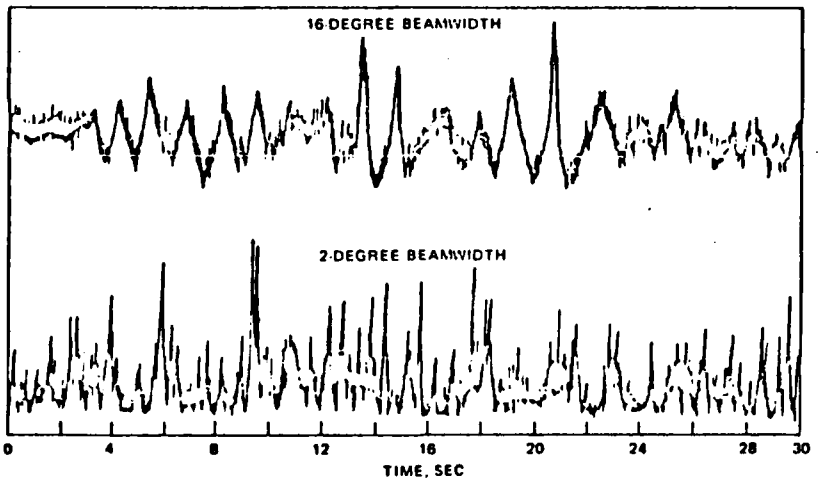

Fig. 20 Raw Reflectance Data [Ref. 13]

Variations in windspeed during the measurements had a noticable effect on the reflectivity. However, the

functional dependence was difficult to deduce. The consistency of the calculated with the measured data lends credence to the dependence shown in Figure 16. The effects of windspeed decreases considerably for values above about 8 m/s (~ 16 kts). This is about the point at which whitecaps form and therefore must be taken into account.

B. DIFFUSE REFLECTION

A perfectly diffuse reflector results in a Lambertian distribution of reflected power. That is, the light intensity varies as the cosine of the angle from the normal and reflects into a 2π solid angle (hemisphere). The power reflected into the differential solid angle $d\Omega_r$ is

$$dP_r = \rho P_t \, d\Omega_r \frac{P_t \, d\Omega_r \cos(\beta)}{\pi} .$$

Measurements conducted by Stephens and Burroughs [Ref. 5] determined the diffuse reflectivity of sea foam to be about $\rho = .4 \cos(\beta)$. A ship's bow and propeller wake as well as salt water spray from a fire hose were used to simulate whitecaps on the ocean surface. This value of diffuse reflectivity is valid for an ocean surface completely covered with spray; i.e., greater than 60 knots windspeed. The size of water droplets due to the sea spray will be on the order of or larger than the wavelength of the light. The spherical particles can act as partial

reflectors which increase the amount of back reflection during high sea states.

For lesser windspeeds, only a fraction of the surface is covered with whitecaps. The total reflectivity is then the sum of specular and diffuse components. Stephens and Burroughs calculated the total effective diffuse reflectivity (due to specular and diffuse reflection) as a function of angle of incidence with windspeed as a parameter. Their results are shown in Figure 21. The reference value of 0 dB is for a 100% diffuse reflector. The diffuse contribution begins to dominate above about 30 knots windspeed.

The value of $\rho = r R_f / \Omega_t$ can be obtained from Figure 20 and used in the trade off equation for performance predictions for high sea states. Figures 16 and 17 can be used for low sea states. A worst case design value is about -10 dB. The effect of beam pattern is reduced at an altitude of 150 m except for a very narrow beam or an angle of incidence greater than 10^{o}. A fan shaped beam may provide a strong return signal more often than a pencil beam but at lower peak values.

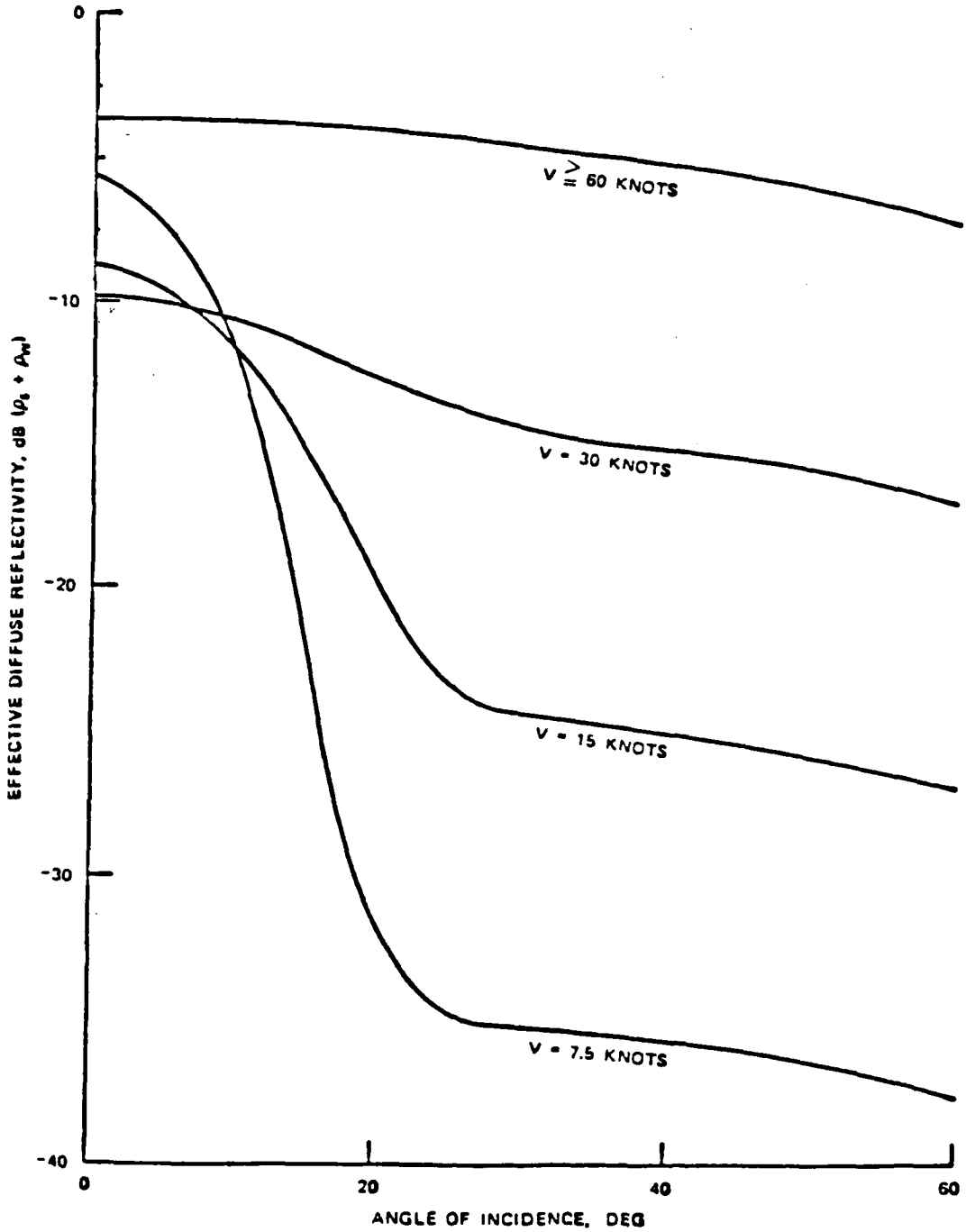

Effective Diffuse Reflectivity as Function of Incidence Angle With Wind Velocity, V, as Parameter. (U)

Fig. 21

IV. PROTOTYPE

Confirmation of theoretical predictions by experiment can validate the theory or indicate deficiences. The next step in development of the laser altimeter was construction of a prototype model for experimental tests. Figure 22 depicts the system that was built and tested both in the laboratory and in the field. The parameters chosen for the design were not "ideal" but were within practical limits set by parts availability and test requirements; i.e., validation of the trade-off equation. A list of parts and costs is presented in the appendix.

A. CONSTRUCTION

The transmitter consists of a laser diode, pulser, and beam-forming optics. Laser output power was selected on the high side at 120 watts. Less power might not have given a useful return signal and greater power was considered uneconomical. Pulse length was set at 75 nsec as a compromise between accuracy and signal strength. An off-the-shelf pulser was used for the initial tests. A cylindrical lens was used to condense the beam to a 3^{o} x 17^{o} pattern. The divergence was measured using an IR image converter. Since the beam does not have sharp, well-defined edges, the measurement is considered approximate. A shield

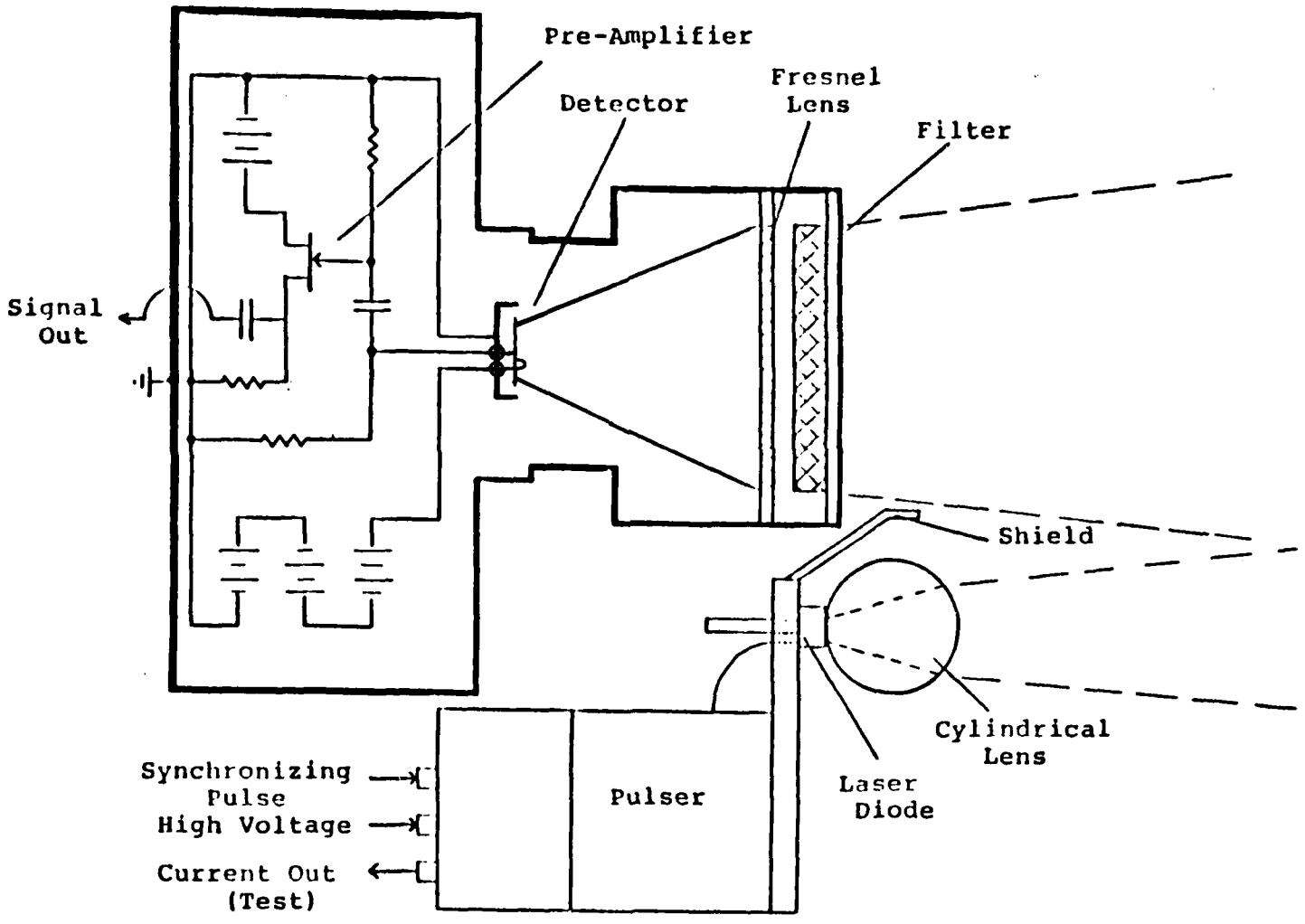

Figure 22. Prototype System

between the output lens and the receiver aperture was needed to block stray light signals.

Both receiver configurations shown in Figure 4 were initially constructed for tests. The first design used a 4-inch diameter Fresnel lens with a 2.8-inch focal length in front of a 2-inch diameter filter. Signal levels, however, were only marginally higher than for the second design which used a 2-inch diameter Fresnel lens behind a 2-inch diameter filter. See Figure 22. The Fresnel lens has a focal length of 2 inches which gives a 12.6^{o} conical field-of-view for the detector selected. Original requirements were for consistent return signals over a wide range of incident angles. This would require a wide beam pattern and large field-of-view. Subsequent specifications of the operational characteristics allowed a smaller beam size for stronger, although less consistent, return signal. The current model was still considered useful for analysis.

The detector is a planar diffused silicon photodiode of 1 cm^{2} area. Responsivity is rated at .4 amps/watt with a capacitance of 200 picofarads. Response time is about 25 nsec. Thus, the detector bandwidth is about 10 MHz. The reverse bias voltage is 67.5 V and the load resistance is 50 kΩ.

A decoupling capacitor of 820 pf is used to separate the signal pulse from the dc component. This high-pass filter has a frequency cutoff of f_c 1/2πRC 4 kHz. From

Chapter II, the post-detection bandwidth should be as small as possible and still pass the signal. The pre-amp uses a single FET with a bandwidth of 500 kHz. The effect of this is to increase the signal rise time to the amplifier to about 300 nsec. This may also limit the signal level to the amplifier. Thermal noise is then about 20 μV.

Total costs for parts is less than $600. This is reasonably inexpensive compared to rangefinders on the open market. Additional costs will be incurred due the items not covered here such as the case, nose dome, batteries, etc. This also does not include the pulser which will need to be designed. However, costs may be reduced through bulk rate buys and/or using different parts; i.e., switching to a 90 watt laser would save over $100.

B. TESTS

Table I contains a summary of the specifications for the prototype. These values, when used in the trade-off equation, should yield signal levels which can be verified by an operational test. Actual time/distance measurements will not be conducted until a further stage of development.

1. Laboratory Test

The first test was conducted in the laboratory using a plate glass window for reflection. The distance was 25 feet. For an index of refraction of the glass of 1.5, the Fresnel reflectance is .04 . This applies for each

air/glass interface (front and rear) for a total of $r = .08$. The reflection factor, R_f can be determined by geometric optics. The power received from specular reflection is

$$P = \frac{P_t \, r \, A}{4 \, \Omega_t \, h^2} \quad .$$

Therefore, by comparison to EQ. 2, $R_f = .25$. The predicted signal voltage is then 420 millivolts. The observed signal was 29 mV.

Many factors can contribute to this discrepancy. Column one of Table 1 shows the values used to predict the signal level by the trade-off equation. Column two shows derated values which, when used in the trade-off equation, yield the observed voltage. Each derated adjustment can be considered as going from an ideal value to a realistic one.

The laser diode is rated at 120 watts by the manufacturer. This is for the maximum current specified under ideal conditions. Output from the pulser may not match these conditions so the power is derated to 100 watts. The product $P_t \tau$ is the energy of the pulse. The pulse length of 75 nsec was obtained from measurements of the current pulses from the laser pulser during operation. It does not take into account the threshold current required to start the laser, which is 25% of the peak current [Ref. 6].

The time to reach the threshold current should be subtracted from the pulse length and then again for the time after it falls below threshold. Thus, the pulse length is derated to $\tau = 50$ nsec.

Transmitter and receiver optics assume a 4% loss at each air/lens interface. This is correct only for light rays at normal incidence. Both the cylindrical and Fresnel lenses have large angular refractions for light rays off the beam axis. Actual losses are not known but have been estimated as shown in Table 1.

The beam pattern was measured visually with an IR converter. The small angular width of the beam was difficult to measure accurately. The 3^{o} spread was derated to 4^{o}. Also the output beam from the laser is not of a spatially uniform power distribution. The laser is a linear array of diodes which produce a rectangular beam. Power density varies along one axis such that peak intensity occurs on either side of the beam center. For normal incidence onto a plate glass window, the power reflected back to the aperture is from the center of the beam where the power density is less than the peak value. This is accounted for by derating the reflection factor, R_f to .15 . Changing the angle of incidence to match the peak power density would require an increased value of R_f.

Although the wide angular spread of the beam (17^{o} is greater than the receiver field of view, it does not

affect the reflection factor for the plate glass target. This is because there is no signal returned at large angles, but only from the small solid angle determined by the image of the aperture in the window. This would not be true for sea surface reflection.

Capacitance of the detector varies slightly with each unit. The value of 200 picofarads is near a typical value listed by the manufacturer. This was increased to 250 pf, the maximum value listed.

These derated values may be closer to the actual values of the system. The problem with a system test is that no indication is given as to which parameter is the most in error or which are correctible. One source of error which does not show up here is due to the frequency response of the detector and pre-amp. A wider bandwidth will pass more signal but will also pass more noise. Timing accuracy also requires a wide bandwidth. Plans for the next stage of development include a second test model with wider bandwidth processing.

A further test of the prototype system was an extension to field conditions. All parameters within the trade-off equation remained the same except for those in the reflection term, $\rho R_f/\Omega_t h^2$.

2. Field Test

The field test was made from the Parrots Ferry bridge over the New Melones reservoir near Columbia, CA. Bridge supports were far enough away from center so as not to be within the beam divergence angle. Height above the water surface was 120 feet. Wind speed was about 10 knots with mostly sunny skies.

Noise measurements were taken with the receiver pointed at the water surface in a direction away from the sun, directly into the glint spot produced by the sun on the water, and at a cloud overhead. Average noise level was about 45 μV for all conditions. Using the derated values, a signal level of .28 mV was predicted. The observed value was .27 mV. This indicates that the overall error in the trade-off equation is the same for each condition. The reflection factor was estimated from Figure 14 as 7 and derated to 5 to account for the transmitter beamwidth/receiver field-of-view mismatch.

Extension of the current system to the nominal altitude of 150 meters yields a predicted return signal below the noise level. However, narrowing the beam divergence and matching the receiver field-of-view yields the predicted signal levels shown in columns (4) and (5) of Table 1. The fan shaped beam does not appear to be nearly as good as the pencil beam if only signal level is considered, but the

return signal would be more consistent for the fan-shaped beam. Analysis in the next stage of development should determine which beamwidth is more appropriate.

TABLE 1. PREDICTED AND MEASURED TEST PARAMETERS

Parameter	Value for Lab Test	Derated Value	Derated Value for Field	Est. Value Fan	Est. Value Pencil
	(1)	(2)	(3)	(4)	(5)
P_t (W)	120	100	100	100	100
τ (nsec)	75	50	50	50	50
T_t	.9	.75	.75	.75	.75
r	.08	.08	.02	.02	.02
R_f	.25	.15	-	-	-
Ω_t (str)	.015	.027	-	-	
R_f/Ω_t (str)$^{-1}$		-	5	3	3
h (m)	7.6	7.6	36.6	150	150
T_r	.5	.3	.3	.3	.3
f/#	1	1	1	1	1
Ω_{fov} (str)	.0377	.0377	.0377	.00274	.0003
A_d (mm^2)	100	100	100	7.1	.79
R_s (A/W)	.4	.4	.4	.4	.4
C (pf)	200	250	250	250	250
V_{signal} (mV) calculated	420	29	.28	.14	1.24
V_{signal} (mV) observed	29	29	.27	-	-
V_{noise} (μV)	6.2	6.2	45	45	45
SNR	1700	1700	6	3	28

V. CONCLUSION

Design of the laser altimeter is proceeding. The initial stage of development can be summarized by the following:

1) Derivation of the trade-off equation now allows system performance to be predicted and test results to be analyzed.

2) Theoretical and measured data exist for reflection at the sea surface. Values of $\rho = rR_f/\Omega_t$ can be predicted based on sea state and transmitter beam pattern and vary from about 0.1 to 1.0 .

3) A prototype model was constructed for less than $600. This establishes a basis from which improvements can be made, both in cost and performance.

4) Test results indicate a discrepancy between predicted and observed performance by a factor of about 15. Derated parameters can account for the difference. Results are consistent from laboratory to field test conditions.

5) Extrapolation of test conditions to an altitude of 150 meters predicts a SNR or 3 for the fan-shaped beam and a SNR of 28 for the pencil beam.

6) Current design specifications are:

Transmitter	GaAs Laser Diode
Peak Power	120 watts
Wavelength	904 nm
Pulse Width	75 nsec
Pulse Repetition Frequency	1 kHz
Receiver	Silicon P-I-N photodiode
Aperture (diam)	2 inches
Focal Length	2 inches
Filter bandwidth	10 nm
Size (cylindrical)	5 inch diameter
	5 inch length

Weight (estimated)	10 lbs
Range	150 meters
Cost	$500

Much remains to be done. It is recommended that the following specific areas be addressed during the next phase of development.

1) Extension of the trade off equation - The pre-amp and amplifier components should be included. The effect of frequency response on system noise as well as signal should indicate a proper system bandwidth and yield more accurate performance predictions.

2) Analysis of actual vehicle dynamics - This should indicate which is more advantageous; the pencil or the fan-shaped beam pattern.

3) Individual components tests - This will determine more accurately derated values. More effective improvements can then be made.

4) Field tests - An altitude of 150 meters should be used under a variety of sea state conditions. The possibility of signal absorption or false detection from a low cloud layer should be investigated.

5) Other system components should be added (synchronizer, redesigned pulser, amplifier, signal processor) as well as refinement of the current system to include a wide bandwidth pre-amp, nose dome, and battery power supply.

APPENDIX A

PARTS LIST OF MAJOR COST ITEMS

Laser - LD 215, Laser Diode Laboratories	$305
Fresnel Lens - #86004, Industrial Optics Div	28
Filter - S-D10-905R, Corian Corporation	150
Detector - PIN 10 D-I, United Detector Technology	49
Pre-Amplifier Electronics	10
	$542

*Does not include:

Synchronizer/Pulser/Signal Processor Electronics

IR Nose Dome

Container

Batteries

LIST OF REFERENCES

1. Johnson, A. M., Nunez, J., and Bushor, L., "Laser Rangefinders - Today's Military and Industrial Systems," Electro-Optical System Design, March, 1976.

2. Bachman, C. G., Laser Radar Systems and Techniques, Artech House, 1979.

3. The Infrared Handbook, The Environmental Research Institute of Michigan, 1978.

4. The Antenna Laboratory of the Ohio State University Research Foundation Report 1675-8, Surface Reflected Energy Received from a Normally Incident Collimated Beam of Optical Radiation, by J. P. J. W. Swennen, 15 September 1965.

5. Naval Weapons Center Report TP 5871 Part I, Active Optical Sea Surface Reflectivity Measurements, by L. M. Stephens and H. H. Burroughs, September 1974.

6. Laser Diode Laboratories, Inc., Pamphlet LD 874, Single Heterojunction GaAs Laser Diode Arrays LD 200,300,400 Series.

7. Air Force Cambridge Research Laboratories Report TR-74-0003, Atmospheric Attenuation of Laser Radiation From .76 to 31.25 μm, by R. A. McClatchey and J. E. A. Selby, p. 96, 3 January 1974.

8. National Technical Information Service Report TT-69-55102, Atmospheric Transparancy in the Visible and the Infrared, by V. E. Zuev, pp. 92 147, 1970

9. Optical Coatings Laboratory, Inc., Effects of the Variation of Angle of Incidence and Temperature on Infrared Filter Characteristics, May 1967.

10. Goss, M., Laser Receivers, p. 70, Wiley, 1966.

11. Cox, C. and Munk, W., "Measurement of the Roughness of the Sea Surface from Photographs of the Sun's Glitter," Journal of the Optical Society of America, v. 44, pp. 838-850, November 1954.

12. International Mathematical & Statistical Libraries, Inc., The IMSL Library, 1984.

13. Naval Weapons Center Technical Memorandum 2453, Daytime Active Optical Sea Surface Reflectivity Measurements, by L. M. Stephens, September 1974.

INITIAL DISTRIBUTION LIST

1.	Defense Technical Information Center Cameron Station Alexandria, Virginia 22304 6145	2
2.	Library, Code 0142 Naval Postgraduate School Monterey, CA 93943 5100	2
3.	Professor G. E. Schacher, Code 61Sq Chairman, Department of Physics Naval Postgraduate School Monterey, CA 93943 5100	2
4.	Professor A. W. Cooper, Code 61Cr Department of Physics Naval Postgraduate School Monterey, CA 93943-5100	2
5.	Professor E. C. Crittenden, Code 61Ct Department of Physics Naval Postgraduate School Monterey, CA 93943 5100	1
6.	Professor W. G. Rodeback, Code 61Rk Department of Physics Naval Postgraduate School Monterey, CA 93943-5100	1
7.	LT Joseph P. Gillo PATWING 1 Det Diego Garcia FPO, S. F., 96685	1
8.	Commander, Space and Naval Warfare Systems Command ATTN. PDE 107-52 Washington DC, 20368 5100	1

END

FILMED

12-85

DTIC